

---

# Gradient-free variational learning with conditional mixture networks

---

**Conor Heins**<sup>\*†</sup>

VERSES AI Research Lab  
Los Angeles, CA, USA  
Max Planck Institute of Animal Behavior  
Department of Collective Behaviour  
Konstanz, Germany  
conor.heins@verses.ai

**Hao Wu**<sup>†</sup>

VERSES AI Research Lab  
Los Angeles, CA, USA  
hao.wu@verses.ai

**Dimitrije Markovic**<sup>†</sup>

VERSES AI Research Lab  
Los Angeles, CA, USA  
Chair of Cognitive Computational Neuroscience  
Technische Universität Dresden  
Dresden, Germany  
dimitrije.markovic@tu-dresden.de

**Alexander Tschantz**

VERSES AI Research Lab  
Los Angeles, CA, USA  
School of Engineering and Informatics  
University of Sussex  
Brighton, UK  
alec.tschantz@verses.ai

**Jeff Beck**<sup>‡</sup>

Department of Neurobiology  
Duke University  
Durham, NC, USA  
jeff.beck@duke.edu

**Christopher Buckley**<sup>‡</sup>

VERSES AI Research Lab  
Los Angeles, CA, USA  
School of Engineering and Informatics  
University of Sussex  
Brighton, UK  
christopher.buckley@verses.ai

## Abstract

Balancing computational efficiency with robust predictive performance is crucial in supervised learning, especially for critical applications. Standard deep learning models, while accurate and scalable, often lack probabilistic features like calibrated predictions and uncertainty quantification. Bayesian methods address these issues but can be computationally expensive as model and data complexity increase. Previous work shows that fast variational methods can reduce the compute requirements of Bayesian methods by eliminating the need for gradient computation or sampling, but are often limited to simple models. We introduce CAVI-CMN, a fast, gradient-free variational method for training conditional mixture networks (CMNs), a probabilistic variant of the mixture-of-experts (MoE) model. CMNs are composed of linear experts and a softmax gating network. By exploiting conditional conjugacy and Pólya-Gamma augmentation, we furnish Gaussian likelihoods for the weights of both the linear layers and the gating network. This enables efficient variational updates using coordinate ascent variational inference (CAVI), avoiding traditional gradient-based optimization. We validate this approach by training two-layer CMNs on standard classification benchmarks from

---

\*Corresponding author

†Co-first authors

‡Co-senior authors

the UCI repository. CAVI-CMN achieves competitive and often superior predictive accuracy compared to maximum likelihood estimation (MLE) with backpropagation, while maintaining competitive runtime and full posterior distributions over all model parameters. Moreover, as input size or the number of experts increases, computation time scales competitively with MLE and other gradient-based solutions like black-box variational inference (BBVI), making CAVI-CMN a promising tool for deep, fast, and gradient-free Bayesian networks.

## 1 Introduction

Modern machine learning methods attempt to learn functions of complex data (e.g., images, audio, text) to predict information associated with that data, such as discrete labels in the case of classification [Bernardo et al., 2007]. Deep neural networks (DNNs) have demonstrated success in this domain, owing to their universal function approximation properties [Park and Sandberg, 1991] and the soft regularization inherited from stochastic gradient descent learning via back propagation [Amari, 1993]. However, despite its computational efficiency, accuracy, and scalability to increasingly large datasets and models, DNNs trained this way do not provide well calibrated predictions and uncertainty estimates, and practitioners typically utilize post-hoc calibration methods on validation datasets [Wang et al., 2021, Shao et al., 2020]. This limits the applicability and reliability of using DNNs in safety-critical applications like autonomous driving, medicine, and disaster response [Papamarkou et al., 2024], where uncertainty-sensitive decision-making is required.

Bayesian machine learning addresses the issues of poor calibration and uncertainty quantification by offering a probabilistic framework that casts learning model parameters  $\theta$  as a process of inference - namely, calculating a posterior distribution over model parameters, given observed data ( $\mathcal{D} = ((\mathbf{x}_1, \mathbf{y}_1), \dots, (\mathbf{x}_n, \mathbf{y}_n))$ ), using Bayes' rule:

$$p(\theta | \mathcal{D}) = \frac{p(\theta, \mathcal{D})}{p(\theta)} \quad (1)$$

The resulting posterior distribution captures both expectations about model parameters  $\theta$  and their uncertainty. The uncertainty is then incorporated in predictions that are, in principle, well-calibrated to novel datapoints coming from the same set. This probabilistic treatment allows methods like Bayesian neural networks (BNNs) [Hernández-Lobato and Adams, 2015] to maintain the expressiveness of deep neural networks while also encoding uncertainty over network weights and thus the network's predictions. However, these methods are known to come with a significant increase in computational cost and thus scale poorly when applied to large datasets and high-dimensional models [Izmailov et al., 2021].

In this paper we introduce a gradient-free variational learning algorithm for a probabilistic variant of a two-layer, feedforward neural network — the conditional mixture network or CMN — and measure its performance on supervised learning benchmarks. This method rests on coordinate ascent variational inference (CAVI) [Wainwright et al., 2008, Hoffman et al., 2013] and hence we name it CAVI-CMN. We compare CAVI-CMN to maximum likelihood estimation and two other Bayesian estimation techniques: the No U-Turn Sampler (NUTS) variant of Hamiltonian Monte Carlo [Hoffman et al., 2014] and black-box variational inference [Ranganath et al., 2014]. We demonstrate that CAVI-CMN maintains the predictive accuracy and scalability of an architecture-matched feedforward neural network fit with maximum likelihood estimation (*i.e.*, gradient descent via backpropagation), while maintaining full distributions over network parameters and generating calibrated predictions, as measured in relationship to state-of-the-art Bayesian methods like NUTS and BBVI.

We summarize the contributions of this work below:

- Introduce and derive a variational inference scheme for the conditional mixture network, which we term CAVI-CMN. This relies on the use of conjugate priors for the linear experts and Pólya-Gamma augmentation [Polson et al., 2013] for the gating network and the final softmax layer.

- CAVI-CMN matches, and sometimes exceeds, the performance of maximum likelihood estimation (MLE) in terms of predictive accuracy, while maintaining the probabilistic benefits of being Bayesian, like quantifying uncertainty and have low calibration error. This is shown across a suite of 8 different supervised classification tasks (2 synthetic, 6 real).
- CAVI-CMN displays all the benefits explained above while requiring drastically less time to converge and overall runtime than the other state-of-the-art Bayesian methods like NUTS and BBVI.

The rest of this paper is organized as follows: first, we discuss related works include the MoE architecture and existing (Bayesian and non-Bayesian approaches) to fitting these models. We then introduce the probabilistic conditional mixture model and derive a variational inference algorithm for optimizing posterior distributions over its latent variables and parameters. We present experimental results comparing the performance of CAVI-based conditional mixture models with sampling based methods, such as BBVI, NUTS, and traditional MLE based estimation, where gradients of the log likelihood are computed using backpropagation and used to update the network’s parameters. Finally, we discuss the implications of these findings and potential directions for future research.

## 2 Related work

The Mixture-of-Experts (MoE) architecture is a close relative of the CMN model we introduce here. [Jacobs et al. \[1991\]](#) originally introduced MoEs as a way to improve the performance of neural networks by combining the strengths of multiple specialized models [\[Gormley and Frühwirth-Schnatter, 2019\]](#). MoE models process inputs by averaging the predictions of individual learners or experts, where each expert’s output is weighted by a different mixing coefficient before the averaging. The fundamental idea behind MoE is that the input space can be partitioned in such a way that different experts (models) can be trained to excel in different regions of this space, with a gating network determining the appropriate expert (or combination of experts) for each input. This leads to composable (and sometimes interpretable) latent descriptions of arbitrary input-output relationships [\[Eigen et al., 2013\]](#), further bolstered by the MoE’s capacity for universal function approximation [\[Nguyen et al., 2016, Nguyen and Chamroukhi, 2018\]](#). Indeed, the powerful self-attention mechanism employed by transformers has demonstrated the power and flexibility of MoE models [\[Movellan and Gabbur, 2020\]](#). Non-Bayesian approaches to MoE typically rely on maximum likelihood estimation (MLE) [\[Jacobs et al., 1991, Jordan and Jacobs, 1994\]](#), which can suffer from overfitting and poor generalization due to the lack of regularization mechanisms [\[Bishop and Svenskn, 2003\]](#), especially in low data size regimes.

To address these issues, Bayesian approaches to MoE have been developed, which incorporate prior information and yield posterior distributions over model parameters [\[Bishop and Svenskn, 2003, Mossavat and Amft, 2011\]](#). This Bayesian treatment enables the estimation of model evidence (log marginal-likelihood) and provides a natural framework for model comparison and selection [\[Svensén, 2003, Zens, 2019\]](#). Bayesian MoE models offer significant advantages, such as improved robustness against overfitting and a better understanding of uncertainty in predictions. However, they also introduce computational challenges, particularly when dealing with high-dimensional data and complex model structures.

The introduction of the Pólya-Gamma (PG) augmentation technique in [Polson et al. \[2013\]](#) enabled a range of novel and more computationally efficient algorithms for Bayesian treatment of MoE models [\[Linderman et al., 2015, He et al., 2019, Sharma et al., 2019, Viroli and McLachlan, 2019, Zens et al., 2023\]](#). Here we complement these past works, which mostly rest on improving sampling methods with PG augmentation, by introducing a closed-form update rules for MoE’s with linear experts in the form of coordinate ascent variational inference (CAVI).

## 3 Methods

In this section we first motivate the use of conditional mixture models for supervised learning, and then introduce the conditional mixture network (CMN), the probabilistic model whose properties and capabilities we demonstrate in the remainder of the paper.

### 3.1 Conditional mixtures for function approximation

Feedforward neural networks are highly expressive, approximating nonlinear functions through sequences of nonlinear transformations, but the posterior distributions over their weights are intractable, requiring expensive techniques like MCMC or variational inference [MacKay, 1992, Blundell et al., 2015, Daxberger et al., 2021].

We circumvent these problems by focusing on the Mixture-of-Experts (MoE) models [Jacobs et al., 1991], and particularly a variant of MoE that is amenable to gradient-free, CAVI parameter updates. MoEs can be made tractable to gradient-free CAVI when the expert likelihoods are constrained to be members of the exponential family (see Section 2 for more details on the MoE architecture), and when the gating network is formulated in such a way to allow exact Bayesian inference (through lower bounds on the log-sigmoid likelihood [Jaakkola and Jordan, 1997, Bishop and Svenskn, 2003] or Pólya-Gamma augmentation [Polson et al., 2013]).

The MoE can be reformulated probabilistically as a mixture model by introducing a latent assignment variable,  $z^n$ , leading to a joint probability distribution of the form

$$p(Y, Z, \Theta) = p(\theta_{1:K})p(\pi) \prod_{i=1}^N p(y^i | z^i, \theta_{1:K})p(z^i | \pi),$$

where  $y^n$  is an observation,  $\Theta = \{\theta_{1:K}, \pi\}$ ,  $p_k(y^n | \theta_k)$  is the  $k^{\text{th}}$ -component’s likelihood and  $z^n$  is a discrete latent variable that assigns the  $n^{\text{th}}$  datapoint to one of the  $K$  mixture components, i.e.  $p_k(y^n | \theta_k) = p(y^n | z^n = k, \theta_{1:K})$ . For instance, if each ‘expert’ likelihood  $p_k(y^n | \theta_k)$  is a Gaussian distribution, then the MoE becomes a Gaussian Mixture Model, where  $\theta_k = (\mu_k, \Sigma_k)$ .

The problem of learning the model’s parameters, then becomes one of doing inference over the latent variables  $Z$  and parameters  $\Theta$  of the mixture model. However, mixture models are generally not tractable for exact Bayesian inference, so some form of approximation or sampling-based scheme is required to obtain full posteriors over their parameters. However, if each expert (i.e., likelihood distribution) in the MoE belongs to the exponential family, the model becomes *conditionally conjugate*. This allows for derivation of exact fixed-point updates to an approximate posterior over each expert’s parameters. The approach we propose, CAVI-CMN, does exactly this – we take advantage of the conditional conjugacy of mixture models, along with an augmentation trick for the the gating network, to make all parameters amenable to an approximate Bayesian treatment. The conditionally-conjugate form of the model allows us to use coordinate ascent variational inference to obtain posteriors over the weights of both the individual linear experts and the gating network [Wainwright et al., 2008, Hoffman et al., 2013, Blei et al., 2017], without resorting to costly gradient or sampling computations.

Going forward we use the term *conditional mixture networks* (CMN) to emphasize (1) the discriminative nature of proposed application of this approach, where the model is designed to predict an output  $y$  given an input  $x$  and (2) the fact that individual MoE layers can be stacked hierarchically into a feedforward architecture. This makes CMNs particularly suitable for tasks such as supervised classification and regression, where the goal is effectively that of function approximation; predict some output variable  $y$  given input regressors  $x$ .

### 3.2 Conditional mixture network overview

The conditional mixture network maps from a continuous input vector  $\mathbf{x}_0 \in \mathbb{R}^d$  to its label  $y \in \{1, \dots, L\}$ . This is achieved with two layers: a conditional mixture of linear experts, which outputs a joint continuous-discrete latent ( $\mathbf{x}_1 \in \mathbb{R}^h, z_1 \in \{1, \dots, K\}$ ) and a multinomial logistic regression, which maps from the continuous latent  $\mathbf{x}_1$  to the corresponding label  $y$ . The probabilistic mapping can be described in terms of the following operations:

$$\begin{aligned} z_1 &\sim \text{Mult}(z_1; \mathbf{x}_0, \boldsymbol{\beta}_0) \\ \mathbf{x}_1 &= \mathbf{A}_{z_1} \cdot [\mathbf{x}_0; 1] + \mathbf{u}_{z_1}, & \mathbf{u}_{z_1} &\sim N(\mathbf{0}, \boldsymbol{\Sigma}_{z_1}) \\ y &\sim \text{Mult}(y; \mathbf{x}_1, \boldsymbol{\beta}_1) \end{aligned}$$

where we pad the input variable  $\mathbf{x}_0$  with a constant value set to 1, to absorb the bias term within the mapping matrix  $\mathbf{A}_{z_1} \in \mathbb{R}^{h \times d+1}$ , and where  $\text{Mult}(z; \mathbf{x}, \boldsymbol{\beta})$  denotes a multinomial distribution parameterized with a regressor  $\mathbf{x}$  and logistic regression coefficients  $\boldsymbol{\beta}$ . Note that for every pair of

regressors and labels  $(\mathbf{x}_0^n, y^n)$ , we assume a corresponding pair of latent variables  $(\mathbf{x}_1^n, z_1^n)$ . Written in this way, it becomes clear that CMN is a mixture of linear transforms that is capable of modeling non-linear transfer functions via a piecewise linear approximation.

In order to obtain a normally distributed posterior over the multinomial logistic regression weights,  $\beta_0$  and  $\beta_1$ , we use Pólya-Gamma augmentation [Polson et al., 2013, Linderman et al., 2015] applied to the stick breaking construction for the multinomial distribution:

$$p(z = k | \beta, \mathbf{x}) = \pi_k(\beta, \mathbf{x}) \prod_{j=1}^{k-1} (1 - \pi_j(\beta, \mathbf{x}))$$

$$\pi_j(\beta, \mathbf{x}) = \frac{1}{1 + \exp\{-\beta_j \cdot [\mathbf{x}; 1]\}}, \forall j < K$$

$$\pi_K = 1$$
(2)

where for the gating network (input layer) we will have coefficients of dimension  $\beta_0 \in \mathbb{R}^{K-1 \times d}$ , and for the output likelihood coefficients of dimension  $\beta_1 \in \mathbb{R}^{L-1 \times h}$ .

### 3.3 Generative model for the conditional mixture network

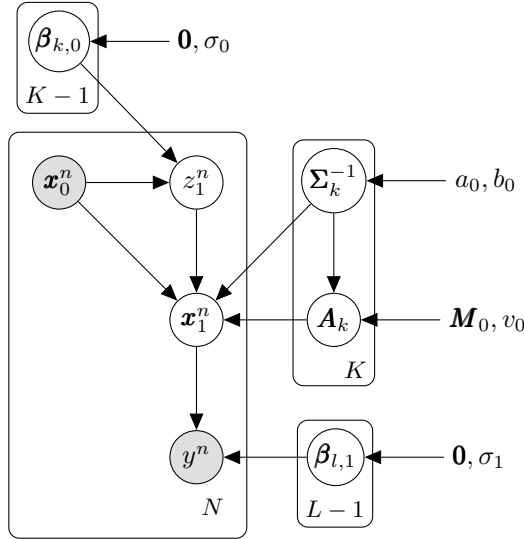


Figure 1: A Bayesian network representation of the two-layer conditional mixture network, with input-output pairs  $\mathbf{x}_0^n, y^n$  and latent variables  $\mathbf{x}_1^n, z_1^n$ . Observations are shaded nodes, while latents and parameters are transparent. Prior hyperparameters are shown without boundaries.

Given a set of labels  $Y = \{y^1, y^2, \dots, y^N\}$ , and regressors  $\mathbf{X}_0 = \{\mathbf{x}_0^1, \mathbf{x}_0^2, \dots, \mathbf{x}_0^N\}$ , that define i.i.d input-output pairs  $\mathbf{x}_0^n, y^n$ , we write the joint distribution over labels  $Y$ , latents  $\mathbf{X}_1, Z_1$ , and parameters  $\Theta$  as:

$$p(\mathbf{Y}, \mathbf{X}_1, Z_1, \Theta | \mathbf{X}_0) = p(\Theta) \prod_{n=1}^N p_{\beta_1}(y^n | \mathbf{x}_1) p_{\lambda_1}(\mathbf{x}_1^n | \mathbf{x}_0^n, z_1^n) p_{\beta_0}(z_1^n | \mathbf{x}_0^n)$$

$$p(\Theta) = p(\beta_1) p(\beta_0) p(\lambda_1)$$

$$= \prod_{l=1}^{L-1} p(\beta_{l,1}) \prod_{k=1}^{K-1} p(\beta_{k,0}) \prod_{j=1}^K p(\mathbf{A}_j, \Sigma_j^{-1})$$
(3)

Note that this model structure, with input and target variables, is often referred to as a *discriminative* model, as opposed to a *generative* model [Bernardo et al., 2007]. However, we use the term generative model to emphasize the fact that the model contains priors over latent variables  $(\mathbf{X}_1, Z_1)$ , and parameters  $\left(\Theta = \left(\beta_{1:L-1,1}, \beta_{1:K-1,0}, \mathbf{A}_{1:K}, \Sigma_{1:K}^{-1}\right)\right)$ , and that we are estimating posteriors

over these quantities, by maximizing a lower bound on marginal likelihood of the observed target variables  $Y$ . Note that going forward, we will sometimes use  $\lambda_1$  as notational shorthand for the parameters  $\mathbf{A}_{1:K}, \Sigma_{1:K}^{-1}$  of the first layer’s linear experts.

We specify the following conditionally conjugate priors for the parameters of the two-layer CMN:

$$\begin{aligned}
p\left(\mathbf{A}_k | \Sigma_k^{-1}\right) &= \mathcal{MN}\left(\mathbf{A}_k; \mathbf{M}_0, \Sigma_k, v_0 \mathbf{I}_{d+1}\right) \\
p\left(\Sigma_k^{-1} \equiv \text{diag}\left(\sigma_k^{-2}\right)\right) &= \prod_{i=1}^h \Gamma\left(\sigma_{k,i}^{-2}; a_0, b_0\right) \\
p\left(\beta_{k,0}\right) &= \mathcal{N}\left(\beta_{k,0}; \mathbf{0}, \sigma_0^2 \mathbf{I}_{d+1}\right) \\
p\left(\beta_{l,1}\right) &= \mathcal{N}\left(\beta_{l,1}; \mathbf{0}, \sigma_1^2 \mathbf{I}_{h+1}\right)
\end{aligned} \tag{4}$$

where we fixed the prior mean matrix of the linear transformation  $\mathbf{A}_k$  to be a matrix of zeros:  $\mathbf{M}_0 = \mathbf{0}$ . In the following section we introduce a mean-field variational inference scheme we use for performing inference and learning in the two-layer CMN.

### 3.4 Coordinate ascent variational inference with conjugate priors

In this section we detail a variational approach for inverting the probabilistic model described in Equation (3) and computing an approximate posterior over latents and parameters specified as

$$p\left(\mathbf{X}_1, \mathbf{Z}_1, \Theta | Y, \mathbf{X}\right) = \frac{p\left(Y, \mathbf{X}_1, \mathbf{Z}_1, \Theta, \mathbf{X}\right)}{p\left(Y | \mathbf{X}\right)} \approx q\left(\Theta\right) \prod_{n=1}^N q\left(z_1^n\right) q\left(\mathbf{x}_1^n | z_1^n\right) \tag{5}$$

where  $q\left(\mathbf{x}_1^n | z_1^n\right)$  corresponds to a component specific multivariate normal distribution, and  $q\left(z_1^n\right)$  to a multinomial distribution. Importantly, the approximate posterior over parameters  $q\left(\Theta\right)$  further factorizes [Svensén, 2003] as

$$\begin{aligned}
q\left(\Theta\right) &= \prod_{l=1}^{L-1} q\left(\beta_{l,1}\right) \prod_{k=1}^{K-1} q\left(\beta_{k,0}\right) \underbrace{\prod_{j=1}^K q\left(\mathbf{A}_j, \Sigma_j^{-1}\right)}_{=q\left(\lambda_1\right)} \\
q\left(\beta_{l,1}\right) &= \mathcal{N}\left(\beta_{l,1}; \boldsymbol{\mu}_{l,1}, \Sigma_{l,1}\right) \\
q\left(\beta_{l,0}\right) &= \mathcal{N}\left(\beta_{l,0}; \boldsymbol{\mu}_{k,0}, \Sigma_{k,0}\right) \\
q\left(\mathbf{A}_j | \Sigma_j^{-1}\right) &= \mathcal{MN}\left(\mathbf{A}_j; \mathbf{M}_j, \Sigma_j, \mathbf{V}_j\right) \\
q\left(\Sigma_j^{-1}\right) &= \prod_{i=1}^h \Gamma\left(\sigma_{i,j}^{-2}; a_j, b_{i,j}\right)
\end{aligned} \tag{6}$$

The above form of the approximate posterior allows us to define tractable conditionally conjugate updates for each factor. This becomes evident from the following expression for the evidence lower-bound (ELBO) on the marginal log likelihood

$$\mathcal{L}(q) = \mathbb{E}_{q\left(\mathbf{x}_1, \mathbf{z}_1\right) q\left(\Theta\right)} \left[ \sum_{n=1}^N \ln \frac{p_{\Theta}\left(y^n, \mathbf{x}_1^n, z_1^n | \mathbf{x}_0^n\right)}{q\left(z_1^n\right) q\left(\mathbf{x}_1^n | z_1^n\right)} \right] + \mathbb{E}_{q\left(\Theta\right)} \left[ \ln \frac{p\left(\beta_1\right) p\left(\beta_0\right) p\left(\lambda_1\right)}{q\left(\beta_1\right) q\left(\beta_0\right) q\left(\lambda_1\right)} \right] \tag{7}$$

We maximize the ELBO using an iterative update scheme for the parameters of the approximate posterior, often referred to as variational Bayesian expectation maximisation (VBEM) [Beal, 2003] or coordinate ascent variational inference (CAVI) [Bishop and Nasrabadi, 2006, Blei et al., 2017]. The procedure consists of two parts:

First, we fix the posterior over the parameters (to randomly initialized values). Given the posterior over parameters, we update the posterior over latent variables (variational E-step) as

$$\begin{aligned}
q_t(\mathbf{x}_1^n | z_1^n) &\propto \exp \left\{ \mathbb{E}_{q_{t-1}(\boldsymbol{\beta}_1) q_{t-1}(\boldsymbol{\lambda}_1)} \left[ \ln p_{\boldsymbol{\beta}_1}(y^n | \mathbf{x}_1^n) + \ln p_{\boldsymbol{\lambda}_1}(\mathbf{x}_1^n | \mathbf{x}_0^n, z_1^n) \right] \right\} \\
q_t(z_1^n) &\propto \exp \left\{ \mathbb{E}_{q_{t-1}(\boldsymbol{\Theta})} \left[ \left\langle \ln p_{\boldsymbol{\beta}_1, \boldsymbol{\lambda}_1}(y^n, \mathbf{x}_1^n | \mathbf{x}_0^n, z_1^n) \right\rangle_{q_t(\mathbf{x}_1^n | z_1^n)} + \ln p_{\boldsymbol{\beta}_0}(z_1^n | \mathbf{x}_0^n) \right] \right\} \quad (8)
\end{aligned}$$

Second, the posterior over latents that was updated in the E-step, is used to update the posterior over parameters (variational M-step) as

$$\begin{aligned}
q_t(\boldsymbol{\beta}_1) &\propto \exp \left\{ \sum_{n=1}^N \mathbb{E}_{q_t(\mathbf{x}_1^n, z_1^n)} \left[ \ln p_{\boldsymbol{\beta}_1}(y^n | \mathbf{x}_1^n) \right] \right\} \\
q_t(\boldsymbol{\beta}_0) &\propto \exp \left\{ \sum_{n=1}^N \mathbb{E}_{q_t(z_1^n)} \left[ \ln p_{\boldsymbol{\beta}_1}(z_1^n | \mathbf{x}_0^n) \right] \right\} \quad (9) \\
q_t(\boldsymbol{\lambda}_1) &\propto \exp \left\{ \sum_{n=1}^N \mathbb{E}_{q_t(\mathbf{x}_1^n, z_1^n)} \left[ \ln p_{\boldsymbol{\lambda}_1}(\mathbf{x}_1^n | z_1^n, \mathbf{x}_0^n) \right] \right\}
\end{aligned}$$

In the variational inference literature, the distinction between latents and parameters is often described in terms of ‘local’ vs ‘global’ latent variables [Hoffman et al., 2013], where local variables are datapoint-specific, and global variables are shared across datapoints. The exact form of the updates to the parameters of the linear experts in Equation (9), i.e.  $q_t(\boldsymbol{\lambda}_1) = q_t(\mathbf{A}_{1:K}, \boldsymbol{\Sigma}_{1:K}^{-1})$  are found in Appendix B.

Importantly, the update equations described in Equation (8) and in the first two lines of Equation (9) are not computationally tractable without an additional approximation, known as Pólya-Gamma augmentation of the multinomial distribution. The full details of the augmentation procedure are described in Appendix A.1. Here we will briefly sketch the main steps and describe the high level, augmented update equations. The Pólya-Gamma augmentation introduces datapoint-specific auxiliary variables  $(\boldsymbol{\omega}_1^n, \boldsymbol{\omega}_0^n)$ , that help us transform the log-probability of the multinomial distribution into a quadratic function [Polson et al., 2013, Linderman et al., 2015] over coefficients  $(\boldsymbol{\beta}_1, \boldsymbol{\beta}_0)$ , and latents  $\mathbf{x}_1^n$ . This quadratic form enables tractable update of  $q(\mathbf{x}_1^n | z_1^n)$  in the form of a multivariate normal distribution, and a tractable updating of posteriors over coefficients  $q(\boldsymbol{\beta}_1)$  and  $q(\boldsymbol{\beta}_0)$ .

With the introduction of the auxiliary variables the variational expectation and maximisation steps are expressed as



Update latents (‘E-step’)

$$\begin{aligned}
q_t(\mathbf{x}_1^n | z_1^n) &\propto \exp \left\{ \mathbb{E}_{q_{t-1}(\boldsymbol{\beta}_1) q_{t-1}(\boldsymbol{\lambda}_1)} \left[ \langle l(y^n, \mathbf{x}_1^n, \boldsymbol{\omega}_1^n, \boldsymbol{\beta}_1) \rangle_{q_{t-1}(\boldsymbol{\omega}_1^n | y^n)} + \ln p_{\boldsymbol{\lambda}_1}(\mathbf{x}_1^n | \mathbf{x}_0^n, z_1^n) \right] \right\} \\
q_t(\boldsymbol{\omega}_1 | y^n) &\propto p(\boldsymbol{\omega}_1^n | y^n) \exp \left\{ \mathbb{E}_{q_{t-1}(\boldsymbol{\beta}_1) q_t(\mathbf{x}_1^n | z_1^n)} [l(y^n, \mathbf{x}_1^n, \boldsymbol{\omega}_1^n, \boldsymbol{\beta}_1)] \right\} \\
q_t(\boldsymbol{\omega}_0 | z_1^n) &\propto p(\boldsymbol{\omega}_0^n | z_1^n) \exp \left\{ \mathbb{E}_{q_{t-1}(\boldsymbol{\beta}_0)} [l(z_1^n, \mathbf{x}_0^n, \boldsymbol{\omega}_0^n, \boldsymbol{\beta}_0)] \right\} \\
q_t(z_1^n) &\propto \exp \left\{ \mathbb{E}_{q_{t-1}(\boldsymbol{\Theta})} \left[ \bar{l}_{z_1^n, t}(y^n, \boldsymbol{\beta}_1) + R_{z_1^n, t}(\mathbf{x}_0^n, \boldsymbol{\lambda}_1) + \bar{l}_t(z_1^n, \mathbf{x}_0^n, \boldsymbol{\beta}_0) \right] \right\}
\end{aligned}$$

Update parameters (‘M-step’)

$$\begin{aligned}
q_t(\boldsymbol{\beta}_1) &\propto \exp \left\{ \sum_{n=1}^N \mathbb{E}_{q_t(\mathbf{x}_1^n, z_1^n) q_t(\boldsymbol{\omega}_1^n | y^n)} [l(y^n, \mathbf{x}_1^n, \boldsymbol{\beta}_1, \boldsymbol{\omega}_1^n)] \right\} \\
q_t(\boldsymbol{\beta}_0) &\propto \exp \left\{ \sum_{n=1}^N \mathbb{E}_{q_t(z_1^n) q_t(\boldsymbol{\omega}_0^n | z_1^n)} [l(z_1^n, \mathbf{x}_0^n, \boldsymbol{\beta}_0, \boldsymbol{\omega}_0^n)] \right\}
\end{aligned} \tag{10}$$

where we omitted terms whose form did not change.  $R_{z_1^n, t}(\mathbf{x}_0^n, \boldsymbol{\lambda}_1)$  reflects a contribution to  $q(z_1^n)$  that depends on the expected log partition of the linear (Matrix Normal Gamma) likelihood  $p_{\boldsymbol{\lambda}_1}(\mathbf{x}_1^n | \mathbf{x}_0^n, z_1^n)$ . Note that the updates to each subset of posteriors (latents or parameters) have an analytic form due to the conditional conjugacy of the model. Importantly, both priors and posterior of the auxiliary variables are Pólya-Gamma distributed [Polson et al., 2013].

Finally, in the above update equations, we have replaced instances of the multinomial distribution  $p(z | \mathbf{x}, \boldsymbol{\beta})$  with its augmented form  $p(\omega | z) e^{l(z, \mathbf{x}, \boldsymbol{\omega}, \boldsymbol{\beta})}$  where the function  $l(\cdot)$  is quadratic with respect to the coefficients  $\boldsymbol{\beta}$  and the input variables  $\mathbf{x}$ , leading to tractable update equations.

## 4 Results

To evaluate the effectiveness of the CAVI-based approach, we compared it to other approximate inference algorithms, using several real and synthetic datasets. We compared CMNs fit with CAVI to the following three approaches:

**MLE** — We obtained point estimates for the parameters  $\mathbf{A}_{1:K}, \boldsymbol{\Sigma}_{1:K}^{-1}, \boldsymbol{\beta}_0, \boldsymbol{\beta}_1$  of the CMN using maximum-likelihood estimation. For gradient-based optimization of the loss function (the negative log likelihood), we used the AdaBelief optimizer with parameters set to its default values as introduced in Zhuang et al. [2020] ( $\alpha = 1e - 3, \beta_1 = 0.9, \beta_2 = 0.999$ ), and run the optimization for 20,000 steps. This implements deterministic gradient descent, not stochastic gradient descent, because we fit the model in ‘full-batch’ mode, i.e., without splitting the data into mini-batches and updating model parameters using noisy gradient estimates.

**NUTS-HMC** — We use the No-U-Turn Sampler (NUTS), an extension to the Hamiltonian Monte Carlo (HMC) samplers, that incorporates adaptive step sizes [Hoffman et al., 2014]. Markov Chain Monte Carlo converges in distribution to samples from a target distribution, so for this method we obtain samples from a joint distribution  $p(\mathbf{A}_{1:K}, \boldsymbol{\Sigma}_{1:K}^{-1}, \boldsymbol{\beta}_0, \boldsymbol{\beta}_1 | Y, \mathbf{X}_0)$  that approximate the true posterior. We used 800 warm-up steps, 16 independent chains, and 64 samples for each chain.

**BBVI** — Black-Box Variational Inference (BBVI) method [Ranganath et al., 2014]. In contrast, to CAVI, the BBVI maximizes evidence lower bound (ELBO) using stochastic estimation of the gradients of variational parameters. While BBVI does not require conjugate relationships in the generative model, we use the same CMN model and variational distributions as we use for CAVI-CMN, in order to ensure fair comparison. For stochastic optimization,



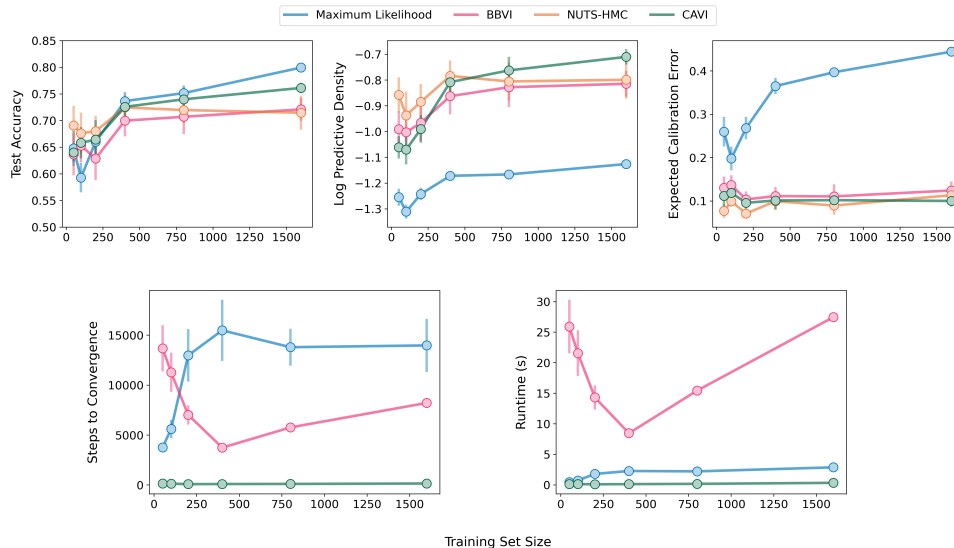


Figure 2: Performance and runtime results of the different inference algorithms on the ‘Pinwheel’ dataset. The standard deviation (vertical lines) of the performance metric is depicted together with the mean estimate (circles) over different runs. The top row of subplots show performance metrics across training set sizes: test accuracy (top left); log predictive density (top center), and expected calibration error (top right). The bottom row shows runtime metrics as a function of increasing training set size: the number of iterations required to achieve convergence (lower left); and the total runtime, estimated using the product of the number of iterations to convergence and the average cost (in seconds) for running one iteration and the average cost (in seconds) for running one iteration (lower right). The number of iterations required for convergence was calculated by determining the number of gradient steps (or M steps, for CAVI) taken before the ELBO (or negative log likelihood, for MLE) reached 95% of its maximum value (see Appendix E for details on how these metrics were computed).

we used the AdaBelief optimizer with learning rate  $\alpha = 5e - 3$  (other hyperparameters same as for MLE), used 8 samples to estimate the ELBO gradient (the `num_particles` argument of the `Trace_ELBO()` class), and ran the optimizer for 20,000 steps).

For the Bayesian methods (CAVI, NUTS, and BBVI), we used the same form for the CMN priors (see Equation (4) for their parameterization) and fixed the prior parameters to the following values, used for all datasets:  $v_0 = 10$ ,  $a_0 = 2$ ,  $b_0 = 1$ ,  $\sigma_0, \sigma_1 = 5$ . For all datasets, we fixed the dimension of the continuous latent  $\mathbf{x}_1$  to be  $h = L - 1$ , where  $L$  is the number of classes. For the Pinwheels dataset (see Section 4.1 below), we set the number of linear experts (and hence the dimension of the discrete latent  $\mathbf{z}_1$ ) to be  $K = 10$ , while for all other datasets we used  $K = 20$ .

#### 4.1 Comparison on synthetic datasets

For synthetic datasets we selected the Pinwheels and the Waveform Domains [Breiman and Stone, 1988] datasets. The pinwheels dataset is a synthetic dataset designed to test the model’s ability to handle nonlinear decision boundaries and data with non-Gaussian densities. The dataset consists of multiple clusters arranged in a pinwheel pattern, posing a challenging task for mixture models [Johnson et al., 2016] due to the curved and elongated spatial distributions of the data. See Appendix C for the parameters we used to simulate the pinwheels dataset. Similarly, the Waveform Domains dataset consists of synthetic data generated to classify three different waveform patterns, where each class is described by 21 continuous attributes [Breiman and Stone, 1988].

We fit all inference methods using different training set sizes, where each next training set was twice as large as the previous (for pinwheels: we trained using train sizes 50 to 1600; for waveform domains: train sizes 60 to 3840). This was done in order to study the robustness of performance in the low data regime. For each training size, we used the same test-set to evaluate performance

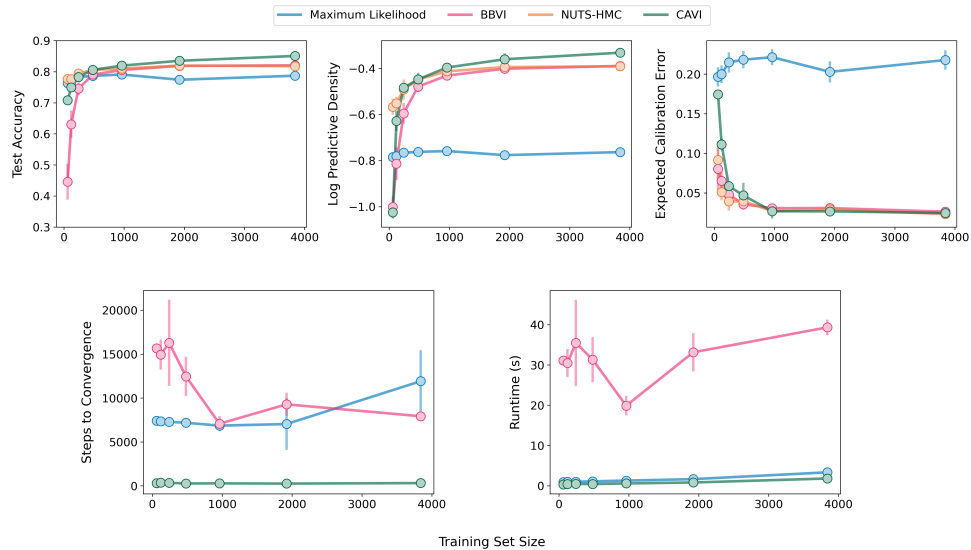


Figure 3: Performance and runtime results of the different models on the ‘Waveform Domains’ dataset. The waveform dataset consists of synthetic data generated to classify three different waveform patterns. Each instance is described by 21 continuous attributes. See [here](#) for more information about the dataset. Descriptions of each subplot are same as in the Figure 2 legend.

(for pinwheels, 500 examples; for waveform domains: 1160 datapoints). For each inference method and examples set size, we fit using the same batch of training data, but with 16 randomly-initialized models (different initial posterior samples or parameters).

We assess the performance of the different inference methods using three main metrics: predictive accuracy (Test Accuracy), log-predictive density (LPD), and expected calibration error (ECE). Log predictive density is a common measure of predictive accuracy for methods that output probabilities [Gelman et al., 2014], and expected calibration error measures how well a model’s predictions are calibrated to the class probabilities observed in the data [Guo et al., 2017]. In Figure 2 we visualize each of these metrics for the Pinwheels dataset and in Figure 3 for the Waveform dataset as a function of training set size. The CAVI-based approach achieves comparable log predictive density and calibration error to the other two Bayesian methods, which all outperform maximum likelihood estimation in LPD and ECE. This holds across training set sizes, indicating better sample efficiency.

## 4.2 Comparison on real-world datasets

To further validate the performance of CAVI-CMN, we conducted experiments using 6 real-world classification datasets from the UCI Machine Learning Repository [Kelly et al., 2024]. Table 1 summarizes the performance of the different algorithms on all 7 different UCI datasets (the Waveform domains dataset and the 6 real datasets), using the widely applicable information criterion (WAIC) as a measure of performance. WAIC is an approximate estimate of leave-one-out cross-validation [Vehtari et al., 2017, Watanabe and Opper, 2010].

The CAVI-CMN approach consistently provided higher WAIC scores compared to the MLE algorithm, and WAIC scores that were on par with BBVI and NUTS. The results confirm that using fully conjugate priors within the CAVI framework does not diminish the inference and the predictive performance of the algorithm, when compared to the state-of-the-art Bayesian methods such as NUTS and BBVI. Importantly, CAVI-CMN offers substantial advantages in terms of computational efficiency, as explored in the next section.

	Rice	Breast Cancer	Waveform	Vehicle Silh.	Banknote	Sonar	Iris
CAVI	-0.1820	-0.0504	<b>-0.2921</b>	<b>-0.3281</b>	-0.0206	-0.1544	-0.0747
MLE	-0.3599	-0.3133	-0.5759	-0.7437	-0.3133	-0.3133	-0.5514
NUTS	<b>-0.1278</b>	<b>-0.0324</b>	-0.3753	-0.3767	<b>-0.0110</b>	<b>-0.0306</b>	<b>-0.0413</b>
BBVI	-0.1739	-0.0763	-0.3618	-0.4154	-0.0382	-0.0583	-0.1544

Table 1: Comparison of widely-applicable information criterion (WAIC) for different methods evaluated on 7 different UCI datasets. The highest WAIC score for each dataset is highlighted in bold-face.

### 4.3 Runtime comparison

The NUTS algorithm, although considered state-of-the-art in terms of inference robustness and accuracy (for well calibrated models [Gelman et al., 2020]), is notoriously difficult to apply to large-scale problems [Cobb and Jalaian, 2021]. Hence, the preferred algorithm of choice for probabilistic machine learning applications have been methods grounded in variational inference, such as black-box variational inference (BBVI) [Ranganath et al., 2014] and stochastic variational inference (SVI) [Hoffman et al., 2013].

In this subsection, we analyze the runtime efficiency of the MLE and BBVI algorithms for CMN models, in comparison to a CAVI-based approach. The focus is on comparing the computation time as the number of parameters increases along different components of the model.

To ensure comprehensive comparison, we varied the complexity of the models by adjusting the number of components, the dimensionality of the input space, and the number of datapoints. These modifications effectively increase the number of parameters allowing us to observe how each algorithm scales with model complexity.

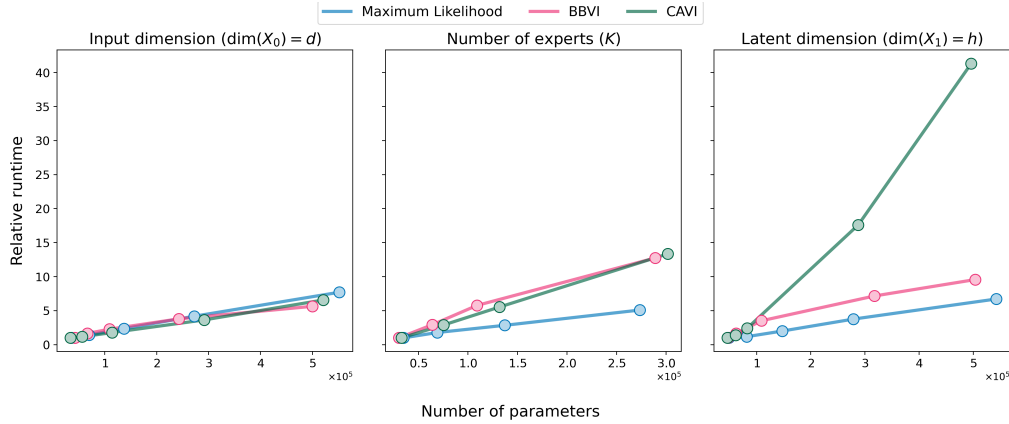


Figure 4: Relative scaling of fitting time in seconds for Maximum Likelihood, BBVI, and CAVI, as a function of the number of parameters. The number of parameters itself was manipulated in three illustrative ways: changing the input dimension  $d$ , changing the number of linear experts  $K$  in the conditional mixture layer, and changing the dimensionality of the continuous latent variable  $h$ .

The runtime performance for varying dataset size on Pinwheel dataset is summarized in the bottom two subplots of Figure 2 which shows the runtime in seconds, and steps until convergence for different algorithms. We used the steps until convergence to assess the runtime for each algorithm. As expected, all algorithms exhibit an increase in runtime as the number of training data increases (which also scales the number of parameters for BBVI and CAVI). However the rate of increase varies significantly across different algorithms, with CAVI-CMN approach showing the best scaling behavior.

Similarly, in Figure 4 we plot the relative runtimes of Maximum Likelihood, CAVI, and BBVI (proportional to the runtime of the least complex variant), as we increase the number of parameters along different elements of CMN. This shows how fitting CMNs with CAVI scales competitively with gradient-based methods like BBVI and Maximum Likelihood Estimation. However, the right-

most subplot indicates that as we increase the dimensionality of the latent variable  $\mathbf{X}_1$ , CAVI-CMN scales more dramatically than the other two methods. This inherits from the computational overhead of matrix operations required by storing multivariate Gaussians posteriors over each continuous latent, i.e.,  $q(\mathbf{x}_1^n | z_1^n) = \mathcal{N}(\mathbf{x}_1^n; \boldsymbol{\mu}_1^n, \boldsymbol{\Sigma}_1^n)$ . Running the CAVI algorithm involves operations (like matrix inversions and matrix-vector products) whose (naive) complexity is quadratic in matrix size. This explains the nonlinear scaling of runtime as a function of  $h$ , the dimension of  $\mathbf{X}_1$ . There are several ways to address this issue:

- **Low-Rank Approximations:** One might use low-rank approximations to the covariance matrix  $\boldsymbol{\Sigma}_1^n$  (e.g., Cholesky or eigendecompositions).
- **Diagonal Covariance Structure:** Further constrain the covariance structure of  $q(\mathbf{x}_1^n)$  by forcing the latent dimensions to be independent in the posterior, i.e.,  $q(\mathbf{x}_1^n | z_1^n) = \prod_{i=1}^h \mathcal{N}(x_{i,1}^n; \mu_{i,1}^n, (\sigma_{i,1}^n)^2)$ . This would then mean that the number of parameters to store would only grow as  $K(2h)$  in the size of the dataset, rather than as  $K(h + O(h^2))$ .
- **Full Mean-Field Approximation:** Enforce a full mean-field approximation between  $\mathbf{X}_1$  and  $Z_1$ , so that one only needs to store  $q(\mathbf{x}_1^n)q(z_1^n)$  rather than  $q(\mathbf{x}_1^n | z_1^n)q(z_1^n)$ . This would reduce the number of multivariate normal parameters that would have to be stored and operated upon by a factor of  $K$ .
- **Shared Conditional Covariance Structure:** Assume that the conditional covariance structure is shared across all training data points, i.e.,  $\boldsymbol{\Sigma}_1^n = \boldsymbol{\Sigma}_1$ , for all  $n \in \{1, 2, \dots, n\}$ .

All of these adjustments would help mitigate the quadratic runtime scaling of CAVI-CMN as the latent dimension  $h$  increases.

In summary, both sets of runtime analyses (both absolute and relative) suggest CAVI-CMN may be an attractive alternative to BBVI suitable for large-scale and time-sensitive applications, which similarly offers a fully Bayesian treatment of latent variables and parameters, while maintaining fast absolute runtime and time-to-convergence.

## 5 Conclusion

We demonstrate that the CAVI-based approach for conditional mixture networks (CMN) significantly outperforms the traditional maximum likelihood estimation (MLE) based approach, in terms of predictive performance and calibration. The improvement in probabilistic performance over the MLE based approaches can be attributed to implicit regularisation via prior information, and proper handling of posterior uncertainty over latent states and parameters, leading to a better representation of the underlying data, reflected in improved calibration error and log predictive density, even in low data regimes.

One of the key advantages of the CAVI-based approach is its computational efficiency compared to the other Bayesian inference methods such as Black-Box variational inference and the No-U-turn sampler (NUTS). While NUTS can sample from the full joint posterior distribution, which maximizes performance in terms of inference quality, this comes at the expense of substantial computational resources, especially for high dimensional and complex models [Hoffman et al., 2013]. The variational methods offer a scalable alternative to this answer, in the form of methods like black-box variational inference (BBVI). Although BBVI is highly efficient in comparison to NUTS, it takes longer to converge than CAVI when applied to CMN. Hence, we expect CAVI to be a more practical choice for large-scale application, especially when further combined with data mini-batching methods [Hoffman et al., 2013].

The benchmark results show that CAVI-CMN algorithm achieves comparable performance to BBVI and NUTS in terms of predictive accuracy, log-predictive density and expected calibration error, while being significantly faster. This balance between predictive likelihood and calibration (jointly viewed as indicators of sample efficiency) is particularly important in real-world applications where robust prediction, reflective of underlying uncertainty, are crucial.

Furthermore, a straightforward mixture of linear components present in CMN, offers additional interoperability benefits. By using the conditionally conjugate priors, and a corresponding mean-field approximation over latent variables and model parameters, we facilitate easier interpretation

of the model parameters and their uncertainties. This is particularly valuable in domains where understanding the underlying data-generating process is as important as the predictive performance, such as in healthcare, finance, and scientific research. Another important point is that the conjugate form of the CMN means that variational updates end up resembling sums of sufficient statistics collected from the data; this means the CAVI algorithm we described is readily amenable to online computation and minibatching, where sufficient statistics can be computed and summed on-the-fly to update model parameters in a streaming fashion [Hoffman et al., 2013]. This approach will become necessary when scaling CAVI-CMN to deeper (more than two-layer) models [Viroli and McLachlan, 2019] and larger datasets, where storing all the sufficient statistics of the data in memory becomes prohibitive.

Overall, these findings underscore the practical advantages of CAVI-CMN and highlight its promise as a new tool for fast probabilistic machine learning.

## Code availability

The code for using CAVI and the other 3 methods to fit the CMN model on the pinwheel and UCI datasets, is available from the `cavi-cmn` repository, which can be found at the following link: <https://github.com/VersesTech/cavi-cmn>.

## Acknowledgments and Disclosure of Funding

The authors would like to thank the members of the VERSES Machine Learning Foundations group for critical discussions and feedback that improved the quality of this work, with special thanks to Tommaso Salvatori, Tim Verbelen, Magnus Koudahl, Toon Van de Maele, Hampus Linander, and Karl Friston.

## References

- Rice (Cammeeo and Osmancik). UCI Machine Learning Repository, 2019. DOI: <https://doi.org/10.24432/C5MW4Z>.
- Shun-ichi Amari. Backpropagation and stochastic gradient descent method. *Neurocomputing*, 5 (4-5):185–196, 1993.
- Matthew James Beal. *Variational algorithms for approximate Bayesian inference*. University of London, University College London (United Kingdom), 2003.
- JM Bernardo, MJ Bayarri, JO Berger, AP Dawid, D Heckerman, AFM Smith, and M West. Generative or discriminative? getting the best of both worlds. *Bayesian statistics*, 8(3):3–24, 2007.
- Christopher M Bishop and Nasser M Nasrabadi. *Pattern recognition and machine learning*, volume 4. Springer, 2006.
- Christopher M. Bishop and Markus Svenskn. Bayesian hierarchical mixtures of experts. In *UAI'03 Proceedings of the Nineteenth conference on Uncertainty in Artificial Intelligence*, pages 57–64. Morgan Kaufmann Publishers Inc., 2003. ISBN 0-127-05664-5.
- David M Blei, Alp Kucukelbir, and Jon D McAuliffe. Variational inference: A review for statisticians. *Journal of the American statistical Association*, 112(518):859–877, 2017.
- Charles Blundell, Julien Cornebise, Koray Kavukcuoglu, and Daan Wierstra. Weight uncertainty in neural network. In *International conference on machine learning*, pages 1613–1622. PMLR, 2015.
- L. Breiman and C.J. Stone. Waveform Database Generator (Version 1). UCI Machine Learning Repository, 1988. DOI: <https://doi.org/10.24432/C5CS3C>.
- Adam D Cobb and Brian Jalaian. Scaling hamiltonian monte carlo inference for bayesian neural networks with symmetric splitting. In *Uncertainty in Artificial Intelligence*, pages 675–685. PMLR, 2021.

- Erik Daxberger, Agustinus Kristiadi, Alexander Immer, Runa Eschenhagen, Matthias Bauer, and Philipp Hennig. Laplace redux-effortless bayesian deep learning. *Advances in Neural Information Processing Systems*, 34:20089–20103, 2021.
- Daniele Durante and Tommaso Rigon. Conditionally Conjugate Mean-Field Variational Bayes for Logistic Models. *Statistical Science*, 34(3):472 – 485, 2019. doi: 10.1214/19-STS712. URL <https://doi.org/10.1214/19-STS712>.
- David Eigen, Marc’ Aurelio Ranzato, and Ilya Sutskever. Learning factored representations in a deep mixture of experts. *arXiv preprint arXiv:1312.4314*, 2013.
- Andrew Gelman, Jessica Hwang, and Aki Vehtari. Understanding predictive information criteria for bayesian models. *Statistics and computing*, 24:997–1016, 2014.
- Andrew Gelman, Aki Vehtari, Daniel Simpson, Charles C Margossian, Bob Carpenter, Yuling Yao, Lauren Kennedy, Jonah Gabry, Paul-Christian Bürkner, and Martin Modrák. Bayesian workflow. *arXiv preprint arXiv:2011.01808*, 2020.
- Isobel Claire Gormley and Sylvia Frühwirth-Schnatter. Mixture of experts models. In *Handbook of mixture analysis*, pages 271–307. Chapman and Hall/CRC, 2019.
- Chuan Guo, Geoff Pleiss, Yu Sun, and Kilian Q Weinberger. On calibration of modern neural networks. In *International conference on machine learning*, pages 1321–1330. PMLR, 2017.
- Jingyu He, Nicholas G Polson, and Jianeng Xu. Data augmentation with polya inverse gamma. *arXiv preprint arXiv:1905.12141*, 2019.
- José Miguel Hernández-Lobato and Ryan Adams. Probabilistic backpropagation for scalable learning of bayesian neural networks. In *International conference on machine learning*, pages 1861–1869. PMLR, 2015.
- Matthew D Hoffman, David M Blei, Chong Wang, and John Paisley. Stochastic variational inference. *Journal of Machine Learning Research*, 2013.
- Matthew D Hoffman, Andrew Gelman, et al. The no-u-turn sampler: adaptively setting path lengths in hamiltonian monte carlo. *J. Mach. Learn. Res.*, 15(1):1593–1623, 2014.
- Pavel Izmailov, Sharad Vikram, Matthew D Hoffman, and Andrew Gordon Gordon Wilson. What are bayesian neural network posteriors really like? In *International conference on machine learning*, pages 4629–4640. PMLR, 2021.
- TS Jaakkola and MI Jordan. Bayesian parameter estimation through variational methods. *Statistics and Computing*, 1997.
- Robert A Jacobs, Michael I Jordan, Steven J Nowlan, and Geoffrey E Hinton. Adaptive mixtures of local experts. *Neural computation*, 3(1):79–87, 1991.
- Matthew J Johnson, David K Duvenaud, Alex Wiltschko, Ryan P Adams, and Sandeep R Datta. Composing graphical models with neural networks for structured representations and fast inference. *Advances in neural information processing systems*, 29, 2016.
- Michael I Jordan and Robert A Jacobs. Hierarchical mixtures of experts and the em algorithm. *Neural computation*, 6(2):181–214, 1994.
- Markelle Kelly, Rachel Longjohn, and Kolby Nottingham. The uci machine learning repository, 2024. URL <https://archive.ics.uci.edu>. <https://archive.ics.uci.edu>.
- Scott Linderman, Matthew J Johnson, and Ryan P Adams. Dependent multinomial models made easy: Stick-breaking with the pólya-gamma augmentation. *Advances in neural information processing systems*, 28, 2015.
- Volker Lohweg. Banknote Authentication. UCI Machine Learning Repository, 2013. DOI: <https://doi.org/10.24432/C55P57>.

- David JC MacKay. A practical bayesian framework for backpropagation networks. *Neural computation*, 4(3):448–472, 1992.
- Iman Mossavat and Oliver Amft. Sparse bayesian hierarchical mixture of experts. In *2011 IEEE Statistical Signal Processing Workshop (SSP)*, pages 653–656. IEEE, 2011.
- Javier R Movellan and Prasad Gabbur. Probabilistic transformers. *arXiv preprint arXiv:2010.15583*, 2020.
- Pete Mowforth and Barry Shepherd. Statlog (Vehicle Silhouettes). UCI Machine Learning Repository. DOI: <https://doi.org/10.24432/C5HG6N>.
- Hien D Nguyen and Faicel Chamroukhi. Practical and theoretical aspects of mixture-of-experts modeling: An overview. *Wiley Interdisciplinary Reviews: Data Mining and Knowledge Discovery*, 8(4):e1246, 2018.
- Hien D Nguyen, Luke R Lloyd-Jones, and Geoffrey J McLachlan. A universal approximation theorem for mixture-of-experts models. *Neural computation*, 28(12):2585–2593, 2016.
- Theodore Papamarkou, Maria Skoularidou, Konstantina Palla, Laurence Aitchison, Julyan Arbel, David Dunson, Maurizio Filippone, Vincent Fortuin, Philipp Hennig, Aliaksandr Hubin, et al. Position paper: Bayesian deep learning in the age of large-scale ai. *arXiv preprint arXiv:2402.00809*, 2024.
- Jooyoung Park and Irwin W Sandberg. Universal approximation using radial-basis-function networks. *Neural computation*, 3(2):246–257, 1991.
- Nicholas G Polson, James G Scott, and Jesse Windle. Bayesian inference for logistic models using pólya–gamma latent variables. *Journal of the American statistical Association*, 108(504):1339–1349, 2013.
- Rajesh Ranganath, Sean Gerrish, and David Blei. Black box variational inference. In *Artificial intelligence and statistics*, pages 814–822. PMLR, 2014.
- Terry Sejnowski and R. Gorman. Connectionist Bench (Sonar, Mines vs. Rocks). UCI Machine Learning Repository. DOI: <https://doi.org/10.24432/C5T01Q>.
- Zhihui Shao, Jianyi Yang, and Shaolei Ren. Calibrating deep neural network classifiers on out-of-distribution datasets. *arXiv preprint arXiv:2006.08914*, 2020.
- Archit Sharma, Siddhartha Saxena, and Piyush Rai. A flexible probabilistic framework for large-margin mixture of experts. *Machine Learning*, 108:1369–1393, 2019.
- Christopher M Bishop Markus Svensén. Bayesian hierarchical mixtures of experts. In *To appear in: Uncertainty in Artificial Intelligence: Proceedings of the Nineteenth Conference*, page 1, 2003.
- Aki Vehtari, Andrew Gelman, and Jonah Gabry. Practical bayesian model evaluation using leave-one-out cross-validation and waic. *Statistics and computing*, 27:1413–1432, 2017.
- Cinzia Viroli and Geoffrey J McLachlan. Deep gaussian mixture models. *Statistics and Computing*, 29:43–51, 2019.
- Martin J Wainwright, Michael I Jordan, et al. Graphical models, exponential families, and variational inference. *Foundations and Trends® in Machine Learning*, 1(1–2):1–305, 2008.
- Deng-Bao Wang, Lei Feng, and Min-Ling Zhang. Rethinking calibration of deep neural networks: Do not be afraid of overconfidence. *Advances in Neural Information Processing Systems*, 34: 11809–11820, 2021.
- Sumio Watanabe and Manfred Opper. Asymptotic equivalence of bayes cross validation and widely applicable information criterion in singular learning theory. *Journal of machine learning research*, 11(12), 2010.
- William Wolberg, Olvi Mangasarian, Nick Street, and W. Street. Breast Cancer Wisconsin (Diagnostic). UCI Machine Learning Repository, 1995. DOI: <https://doi.org/10.24432/C5DW2B>.



- Gregor Zens. Bayesian shrinkage in mixture-of-experts models: identifying robust determinants of class membership. *Advances in Data Analysis and Classification*, 13(4):1019–1051, 2019.
- Gregor Zens, Sylvia Frühwirth-Schnatter, and Helga Wagner. Ultimate pólya gamma samplers—efficient mcmc for possibly imbalanced binary and categorical data. *Journal of the American Statistical Association*, pages 1–12, 2023.
- Juntang Zhuang, Tommy Tang, Yifan Ding, Sekhar C Tatikonda, Nicha Dvornek, Xenophon Papademetris, and James Duncan. Adabelief optimizer: Adapting stepsizes by the belief in observed gradients. *Advances in neural information processing systems*, 33:18795–18806, 2020.

## A Variational Bayesian Multinomial Logistic Regression

In this section, we focus on a single multinomial logistic regression model (not in the context of the CMN), but the ensuing variational update scheme derived in Appendix A.4 is applied in practice to both the gating network's parameters  $\beta_0$  as well as those of the final output likelihood for the class label  $\beta_1$ .

### A.1 Stick-breaking reparameterization of a multinomial distribution

Multinomial logistic regression considers the probability that an outcome variable  $y$  belongs to one of  $K$  mutually-exclusive classes or categories. The probability of  $y$  belonging to the  $k^{\text{th}}$  class is given by the categorical likelihood:

$$p(y = k | \mathbf{x}, \beta) = p_k \quad (11)$$

The problem of multinomial logistic regression is to identify or estimate the values of regression coefficients  $\beta$  that explain the relationship between some dataset of given continuous input regressors  $\mathbf{X} = (\mathbf{x}^1, \mathbf{x}^2, \dots, \mathbf{x}^N)$  and corresponding categorical labels  $Y = (y^1, y^2, \dots, y^N)$ ,  $y^n \in 1, 2, \dots, K$ .

We can use a stick-breaking construction to parameterize the likelihood over  $y$  using a set of  $K - 1$  stick-breaking coefficients:  $\boldsymbol{\pi} = (\pi_1, \dots, \pi_{K-1})$ . Each coefficient is parameterized with an input regressor  $\mathbf{x}$ , and a corresponding set of regression weights  $\beta_j$ . Stick-breaking coefficient  $\pi_j$  is then given by a sigmoid transform of the product of the regression weights and the input regressors:

$$\begin{aligned} \pi_j &= \sigma(\beta_j [\mathbf{x}; 1]) , \\ \text{where } \sigma(\beta_j [\mathbf{x}; 1]) &= \frac{1}{1 + \exp\{-\beta_j [\mathbf{x}; 1]\}} , \\ \text{and } \beta_j [\mathbf{x}; 1] &= \sum_{i=1}^d w_{j,i} x_i + a_j . \end{aligned} \quad (12)$$

The outcome likelihood is then obtained via stick breaking transform<sup>4</sup> as follows

$$p_k = \pi_K \prod_{j=1}^{K-1} (1 - \pi_j) = \sigma(\beta_K [\mathbf{x}; 1]) \prod_{j=1}^{K-1} (1 - \sigma(\beta_j [\mathbf{x}; 1])) = \prod_{j=1}^{K-1} \frac{\exp\{\beta_j [\mathbf{x}; 1]\}}{1 + \exp\{\beta_j [\mathbf{x}; 1]\}} \quad (13)$$

where  $\pi_K = 1$ , and  $\beta_K = \vec{0}$ .

Finally, we can express the likelihood in the form of a Categorical distribution as

$$\text{Cat}(y; \mathbf{x}, \beta) = \prod_{k=1}^{K-1} \frac{(\exp\{\beta_k [\mathbf{x}; 1]\})^{\delta_{k,y}}}{(1 + \exp\{\beta_k [\mathbf{x}; 1]\})^{N_{k,y}}} . \quad (14)$$

where  $N_{k,y} = 1$  for  $k \leq y$ , and  $N_{k,y} = 0$  otherwise (or  $N_{k,y} = 1 - \sum_{j=1}^{k-1} \delta_{j,y}$ ), and  $\delta_{k,y} = 1$  for  $k = y$  and is zero otherwise.

### A.2 Pólya-Gamma augmentation

The *Pólya-Gamma augmentation* scheme [Polson et al., 2013, Linderman et al., 2015, Durante and Rigon, 2019] is defined as

---

<sup>4</sup>This blog post has helpful discussion on the stick-breaking form of the multinomial logistic likelihood and provides more intuition behind its functional form.

$$\frac{(e^\psi)^a}{(1+e^\psi)^b} = 2^{-b} e^{\kappa\psi} \int_0^\infty e^{-\omega\psi^2/2} p(\omega) d\omega \quad (15)$$

where  $\kappa = a - b/2$  and  $p(\omega|b, 0)$  is the density of the Pólya-Gamma distribution  $PG(b, 0)$  which does not depend on  $\psi$ . The useful properties of the Pólya-Gamma are the exponential tilting property expressed as

$$PG(\omega; b, \psi) = \frac{e^{-\omega\psi^2/2} PG(\omega; b, 0)}{\mathbb{E}[e^{-\omega\psi^2/2}]} \quad (16)$$

the expected value of  $\omega$ , and  $e^{-\omega\psi^2/2}$  given as

$$\begin{aligned} \mathbb{E}[\omega] &= \int_0^\infty \omega PG(\omega; b, \psi) d\omega = \frac{b}{2\psi} \tanh\left(\frac{\psi}{2}\right), \\ \mathbb{E}[e^{-\omega\psi^2/2}] &= \cosh^{-b}\left(\frac{\psi}{2}\right) \end{aligned} \quad (17)$$

and the Kulback-Leibler divergence between  $q(\omega) = PG(\omega; b, \psi)$  and  $p(\omega) = PG(\omega; b, 0)$  obtained as

$$D_{KL}[q(\omega)||p(\omega)] = -\mathbb{E}[\omega] \frac{\psi^2}{2} + b \ln \cosh\left(\frac{\psi}{2}\right) = -\frac{b\psi}{4} \tanh\left(\frac{\psi}{2}\right) + b \ln \cosh\left(\frac{\psi}{2}\right). \quad (18)$$

We can express the likelihood function in Equation (14) using the augmentation as

$$\begin{aligned} p(y, \boldsymbol{\omega}|\boldsymbol{\psi}) &= p(y|\boldsymbol{\psi}) p(\boldsymbol{\omega}|y, \boldsymbol{\psi}) = \prod_{k=1}^{K-1} 2^{-b_{k,y}} e^{\kappa_{k,y} \psi_k - \omega_k \psi_k^2/2} PG(\omega_k; b_{k,y}, 0) \\ p(y|\boldsymbol{\psi}) &= \prod_{k=1}^{K-1} 2^{-b_{k,y}} e^{\kappa_{k,y} \psi_k} \int_0^\infty e^{-\omega_k \psi_k^2/2} PG(\omega_k; b_{k,y}, 0) d\omega_k \\ p(\boldsymbol{\omega}|y, \boldsymbol{\psi}) &= \prod_{k=1}^{K-1} PG(\omega_k; b_{k,y}, \psi_k) \end{aligned} \quad (19)$$

where  $b_{k,y} \equiv N_{k,y}$ ,  $\kappa_{k,y} = \delta_{k,y} - N_{k,y}/2$ , and  $\psi_k = \boldsymbol{\beta}_k[\mathbf{x}; 1]$ . Given a prior distribution  $p(\boldsymbol{\psi}) = p(\boldsymbol{\beta}) p(\boldsymbol{x})$ , we can write the joint  $p(y, \boldsymbol{\omega}, \boldsymbol{\psi})$  as

$$\begin{aligned} p(y, \boldsymbol{\omega}, \boldsymbol{\psi}) &= p(\boldsymbol{\omega}|y) p(\boldsymbol{\psi}) e^{l(y, \boldsymbol{\psi}, \boldsymbol{\omega})}, \\ l(y, \boldsymbol{\psi}, \boldsymbol{\omega}) &= \sum_{k=1}^{K-1} l_k(y, \psi_k, \omega_k), \\ l_k(y, \psi_k, \omega_k) &= \kappa_{y,k} \psi_k - b_{y,k} \ln 2 - \omega_k \psi_k^2/2. \end{aligned} \quad (20)$$

### A.3 Evidence lower-bound

Given a set of observations  $\mathcal{D} = (y^1, \dots, y^N)$  the augmented joint distribution can be expressed as

$$p(\mathcal{D}, \boldsymbol{\Omega}, \mathbf{X}, \boldsymbol{\beta}) = p(\boldsymbol{\beta}) \prod_{n=1}^N p(\mathbf{x}^n) p(\boldsymbol{\omega}^n | y^n) e^{l(y^n, \boldsymbol{\psi}^n, \boldsymbol{\omega}^n)}$$

We can express the evidence lower-bound (ELBO) as

$$\begin{aligned}
\mathcal{L}(q) &= E_{q(\boldsymbol{\Omega})q(\mathbf{X})q(\boldsymbol{\beta})} \left[ -\ln q(\boldsymbol{\beta}) + \sum_{n=1}^N \ln \frac{p(y^n, \boldsymbol{\psi}^n, \boldsymbol{\omega}^n)}{q(\boldsymbol{\omega}^n)q(\mathbf{x}^n)} \right] \\
&= E_{q(\boldsymbol{\Omega})q(\mathbf{X})q(\boldsymbol{\beta})} \left[ \ln \frac{p(\boldsymbol{\beta})}{q(\boldsymbol{\beta})} + \sum_{n=1}^N l(y^n, \boldsymbol{\psi}^n, \boldsymbol{\omega}^n) + \ln \frac{p(\boldsymbol{\omega}^n|y^n)}{q(\boldsymbol{\omega}^n)} + \ln \frac{p(\mathbf{x}^n)}{q(\mathbf{x}^n)} \right] \\
&\geq \ln p(\mathcal{D})
\end{aligned} \tag{21}$$

where we use the following forms for the approximate posterior

$$\begin{aligned}
q(\boldsymbol{\Omega}|Y) &= \prod_{n=1}^N q(\boldsymbol{\omega}^n|y^n) = \prod_{n=1}^N \prod_{k=1}^{K-1} PG(b_{k,y^n}, \xi_{k,n}), \\
q(\mathbf{X}) &= \prod_{n=1}^N q(\mathbf{x}^n) = \prod_{n=1}^N \mathcal{N}(\mathbf{x}^n; \boldsymbol{\mu}^n, \boldsymbol{\Sigma}^n), \\
q(\boldsymbol{\beta}) &= \prod_{k=1}^{K-1} \mathcal{N}(\boldsymbol{\beta}_k; \boldsymbol{\mu}_k, \boldsymbol{\Sigma}_k).
\end{aligned} \tag{22}$$

#### A.4 Coordinate ascent variational inference

The mean-field assumption in Equation (22) allows the implementation of a simple CAVI algorithm [Wainwright et al., 2008, Beal, 2003, Hoffman et al., 2013, Blei et al., 2017] which sequentially maximizes the evidence lower bound in Equation (21) with respect to each factor in  $q(\boldsymbol{\Omega}|Y)q(\mathbf{X})q(\boldsymbol{\beta})$ , via the following updates:

Update to latents (‘E-step’)

$$\begin{aligned}
q^{(t,l)}(\mathbf{x}^n) &\propto p(\mathbf{x}^n) \exp \left\{ \mathbb{E}_{q^{(t-1)}(\boldsymbol{\beta})q^{(t,l-1)}(\boldsymbol{\omega}^n)} [l(y^n, \boldsymbol{\psi}^n, \boldsymbol{\omega}^n)] \right\} \\
q^{(t,l)}(\boldsymbol{\omega}_k^n|y^n) &\propto p(\boldsymbol{\omega}_k^n|y^n) \exp \left\{ \mathbb{E}_{q^{(t-1)}(\boldsymbol{\beta})q^{(t,l)}(\mathbf{x}^n)} [l_k(y^n, \boldsymbol{\psi}_k^n, \boldsymbol{\omega}_k^n)] \right\} \\
&\forall n \in \{1, \dots, N\}, \text{ and for } q^{(t,0)}(\boldsymbol{\omega}^n|y^n) = q^{(t-1,L)}(\boldsymbol{\omega}^n|y^n)
\end{aligned} \tag{23}$$

Update to parameters (‘M-step’)

$$q^{(t)}(\boldsymbol{\beta}_k) \propto \exp \left\{ \sum_{n=1}^N \mathbb{E}_{q^{(t)}(\mathbf{x}^n)q^{(t)}(\boldsymbol{\omega}^n|y^n)} [l(y^n, \boldsymbol{\psi}^n, \boldsymbol{\omega}^n)] \right\}$$

at each iteration  $t$ , and multiple local iteration  $l$  during the variational expectation step—until the convergence of the ELBO.

Specifically, the update equations for the parameters of the latents (the ‘E-step’) are:

$$\begin{aligned}
q^{(t,l)}(\mathbf{x}^n) &\propto \mathcal{N}(\mathbf{x}^n; 0, -2\lambda_{2,0}) \exp \left\{ \sum_{k=1}^K \kappa_{k,y^n} \text{Tr} \left( \boldsymbol{\mu}_k^{(t-1)} [\mathbf{x}^n; 1]^T \right) - \frac{\langle \omega_k \rangle}{2} \text{Tr} \left( \mathbf{M}_k^{(t-1)} [\mathbf{x}^n; 1] [\mathbf{x}^n; 1]^T \right) \right\} \\
\lambda_1^{(n,t,l)} &= \sum_{k=1}^{K-1} \left\{ \kappa_{k,y^n} [\boldsymbol{\mu}_k^{(t-1)}]_{1:D} - \langle \omega_k^n \rangle_{t,l-1} [\mathbf{M}_k^{(t-1)}]_{D+1,1:D} \right\} \\
\lambda_2^{(n,t,l)} &= \lambda_{2,0} - \frac{1}{2} \sum_{k=1}^{K-1} \langle \omega_k^n \rangle_{t,l-1} [\mathbf{M}_k]_{1:D,1:D} \\
\mathbf{M}_k^{(t-1)} &= \boldsymbol{\Sigma}_k^{(t-1)} + \boldsymbol{\mu}_k^{(t-1)} [\boldsymbol{\mu}_k^{(t-1)}]^T
\end{aligned} \tag{24}$$

and

$$\begin{aligned}
q^{(t,l)}(\omega_k^n | y^n) &\propto e^{-\omega_k^n \langle \psi_k^2 \rangle / 2} PG(\omega_k^n; b_{k,y^n}, 0) \\
\xi_k^n &= \sqrt{\mathbb{E}_{q^{(t-1)}(\boldsymbol{\beta})} [\psi_k^2]} \\
\xi_k^n &= \sqrt{\text{Tr}(\mathbf{M}_k^{(t-1)} \hat{\mathbf{M}}^{(n,t,l)})} \tag{25}
\end{aligned}$$

where  $\hat{\mathbf{M}}^{(n,t,l)} = \begin{pmatrix} \mathbf{M}^{(n,t,l)} & \boldsymbol{\mu}^{(n,t,l)} \\ [\boldsymbol{\mu}^{(n,t,l)}]^T & 1 \end{pmatrix}$ , and  $\mathbf{M}^{(n,t,l)} = \boldsymbol{\Sigma}^{(n,t,l)} + \boldsymbol{\mu}^{(n,t,l)} [\boldsymbol{\mu}^{(n,t,l)}]^T$ .

Similarly, for the parameter updates ('M-step') we get

$$\begin{aligned}
q^{(t)}(\boldsymbol{\beta}_k) &\propto \mathcal{N}(\boldsymbol{\beta}_k; 0, -2\lambda'_{2,0}) \exp \left\{ \sum_{n=1}^N \kappa_{k,y^n} \text{Tr}(\hat{\boldsymbol{\mu}}^{(n,t)} \boldsymbol{\beta}_k^T) - \frac{\langle \omega_k \rangle_t^n}{2} \text{Tr}(\hat{\mathbf{M}}_i^{(t)} \boldsymbol{\beta}_k \boldsymbol{\beta}_k^T) \right\} \\
\lambda_{k,1}^{(t)} &= \sum_i \kappa_{k,y^n} \hat{\boldsymbol{\mu}}^{(n,t)} \\
\lambda_{k,2}^{(t)} &= \lambda'_{2,0} - \frac{1}{4} \sum_{n=1}^N \frac{b_{k,y^n}}{\xi_k^{(n,t)}} \tanh\left(\frac{\xi_k^{(n,t)}}{2}\right) \hat{\mathbf{M}}^{(n,t)} \tag{26}
\end{aligned}$$

where  $\hat{\boldsymbol{\mu}}^{(n,t)} = [\boldsymbol{\mu}^{(n,t)}; 1]$ .

## B Variational Bayesian Mixture of Linear Transforms

The variational 'M-step' in Equation (9) to update the parameters of the linear experts reduces to a straightforward form when each expert parameterizes a multivariate Gaussian likelihood over the latent variables  $\mathbf{X}_1$  with Matrix Normal Gamma priors over the parameters of the linear function that maps  $\mathbf{X}_0$  to a distribution over  $\mathbf{X}_1$ .

Recall the form of the update to the posterior parameters of the linear experts:

$$q(\mathbf{A}_{1:K}, \boldsymbol{\Sigma}_{1:K}^{-1}) \propto \exp \left\{ \sum_{n=1}^N \mathbb{E}_{q(\mathbf{x}_1^n, z_1^n)} \left[ \ln p(\mathbf{x}_1^n | z_1^n, \mathbf{x}_0^n, \mathbf{A}_{1:K}, \boldsymbol{\Sigma}_{1:K}^{-1}) \right] \right\} \tag{27}$$

The approximate posteriors  $q(\mathbf{A}_{1:K}, \boldsymbol{\Sigma}_{1:K}^{-1})$  and  $q(\mathbf{X}_1, Z_1)$  have the following form:

$$\begin{aligned}
q(\mathbf{A}_{1:K}, \boldsymbol{\Sigma}_{1:K}^{-1}) &= \prod_{k=1}^K \left( \mathcal{MN}(\mathbf{A}_k; \mathbf{M}_k, \boldsymbol{\sigma}_k^{-2} I, \mathbf{V}_k) \prod_{i=1}^h \Gamma(\sigma_{i,k}^{-2}; a_k, b_{i,k}) \right) \\
q(\mathbf{X}_1 | Z_1) &= \prod_{n=1}^N \prod_{k=1}^K \mathcal{N}(\mathbf{x}_1^n; \boldsymbol{\mu}_{k,1}^n, \boldsymbol{\Sigma}_{k,1}^n) \\
q(Z_1) &= \prod_{n=1}^N \text{Cat}(z_1^n; \boldsymbol{\gamma}^n)
\end{aligned}$$

The parameters of the  $k^{\text{th}}$  expert  $q(\mathbf{A}_k, \boldsymbol{\Sigma}_k^{-1})$  can be written in terms of weighted updates to the Matrix Normal Gamma's canonical parameters  $\mathbf{M}_k, \mathbf{V}_k, a_k$  and  $b_k$ :

$$\begin{aligned}
\mathbf{V}_k^{-1} &= \mathbf{V}_{k,0}^{-1} + \sum_{n=1}^N \gamma_k^n \mathbf{x}_0^n (\mathbf{x}_0^n)^\top \\
\mathbf{M}_k &= \left( \mathbf{M}_{k,0} \mathbf{V}_{k,0}^{-1} + \sum_{n=1}^N \gamma_k^n \boldsymbol{\mu}_{k,1}^n (\mathbf{x}_0^n)^\top \right) \mathbf{V}_k \\
a_k &= a_{k,0} + \frac{\sum_{n=1}^N \gamma_k^n}{2} \\
b_{i,k} &= b_{i,k,0} + \frac{1}{2} \left( \sum_{n=1}^N \gamma_k^n \left[ \boldsymbol{\Sigma}_{k,1}^n + \boldsymbol{\mu}_{k,1}^n (\boldsymbol{\mu}_{k,1}^n)^\top \right]_{ii} - \left[ \mathbf{M}_k \mathbf{V}_k^{-1} \mathbf{M}_k^\top \right]_{ii} + \left[ \mathbf{M}_{k,0} \mathbf{V}_{k,0}^{-1} \mathbf{M}_{k,0}^\top \right]_{ii} \right)
\end{aligned} \tag{28}$$

where the notation  $[\cdot]_{ii}$  selects the  $i^{\text{th}}$  element of the diagonal of the matrix in the brackets.

## C Dataset Descriptions

We fit all inference methods using different training set sizes, where each next training set was twice as large as the previous. For each training size, we used the same test-set to evaluate performance. The test set was ensured to have the same relative class frequencies as in the training set(s). For each inference method and examples set size, we fit using the same batch of training data, but with 16 randomly-initialized models (different initial posterior samples or parameters).

### C.1 Pinwheels Dataset

The pinwheels dataset is a synthetic dataset designed to test a model’s ability to handle nonlinear decision boundaries and data with non-Gaussian densities [Johnson et al., 2016]. The structure of the pinwheels dataset is determined by 4 parameters: the number of clusters or distinct spirals; the angular deviation, which defines how far the spiralling clusters deviate from the origin; the tangential deviation, which defines the noise variance of 2-D points within each cluster; and the angular rate, which determines the curvature of each spiral. For evaluating the four methods (CAVI-CMN, MLE, BBVI, and NUTS) on the synthetic pinwheels dataset, we generated a dataset with 5 clusters, with an angular deviation of 0.7, tangential deviation of 0.3 and angular rate of 0.2. We selected these values by looking at the maximum achieved test accuracy across all the methods for different parameter combinations and tried to upper-bound it 80%, which provides a low enough signal-to-noise ratio to be able to meaningfully show differences in probabilistic metrics like calibration and WAIC. For pinwheels, we trained using train sizes 50 to 1600, doubling the number of training examples at each successive training set size. We tested using 500 held-out test examples generated using the same parameters as used for the training set(s).

### C.2 Waveform Domains Dataset

The Waveform Domains dataset consists of synthetic data generated to classify three different waveform patterns, where each class is described by 21 continuous attributes [Breiman and Stone, 1988]. For waveform domains, we fit each model on train sizes ranging from 60 to 3840 examples, and tested on a held-out size of 1160 examples. See [here](#) for more information about the dataset.

### C.3 Vehicle Silhouettes Dataset

This dataset involves classifying vehicle silhouettes into one of four types (bus, van, or two car models) based on features extracted from 2D images captured at various angles [Mowforth and Shepherd]. We fit each model on train sizes ranging from 20 to 650 examples, and tested on a held-out size of 205 examples. See [here](#) for more information about the dataset.

#### C.4 Rice Dataset

The Rice dataset contains measurements related to the classification of rice varieties, specifically Cammeo and Osmancik [mis, 2019]. We fit each model on train sizes ranging from 40 to 2560 examples, and tested on a held-out size of 1250. See [here](#) for more information about the dataset.

#### C.5 Breast Cancer Dataset

The ‘Breast Cancer Diagnosis’ dataset [Wolberg et al., 1995] contains features extracted from breast mass images, which are then used to classify tumors as malignant or benign. See [here](#) for more information about the dataset. We fit each model on train sizes ranging from 25 to 400 examples, and tested on a held-out size of 169.

#### C.6 Sonar (Mines vs Rocks) Dataset

The Sonar (Mines vs Rocks) dataset consists of sonar signals bounced off metal cylinders and rocks under various conditions. The dataset includes 111 patterns from metal cylinders (mines) and 97 patterns from rocks. Each pattern is represented by 60 continuous attributes corresponding to the energy within specific frequency bands [Sejnowski and Gorman]. The task is to classify each pattern as either a mine (M) or a rock (R). For this dataset, we fit each model on train sizes ranging from 8 to 128 examples and tested on a held-out size of 80 examples. See [here](#) for more information about the dataset.

#### C.7 Banknote Authentication Dataset

The ‘Banknote Authentication’ dataset [Lohweg, 2013] contains features extracted from images of genuine and forged banknotes. It is primarily used for binary classification tasks to distinguish between authentic and counterfeit banknotes. See [here](#) for more information about the dataset.

### D UCI Performance Results

In Figures 5 to 9 we report the same performance and runtime metrics as in Figure 2 for 7 UCI datasets, and find that with the exception of the Sonar dataset, CAVI performs competitively with or better than MLE on all datasets, and always outperforms MLE in terms of LPD and ECE. Runtime scaling is similar as reported for the Pinwheels dataset in the main text; CAVI-CMN always converges in fewer steps and is faster than BBVI, and either outperforms or is competitive with MLE in terms of runtime.

### E Model Convergence Determination

For each inference algorithm, the number of iterations taken to converge was determined by running each algorithm for a sufficiently high number of gradient (respectively, CAVI update) steps such that the ELBO (or log likelihood - LL - for MLE) stopped significantly changing. This was determined (through anecdotal inspection over many different initializations and runs across the different UCI datasets) to be 20,000 gradient steps for BBVI, 20,000 gradient steps for MLE, and 500 combined CAVI update steps for CAVI-CMN. To determine the time taken to sufficiently converge, we recorded the value of the ELBO or LL at each iteration, and fit an exponential decay function to the negative of each curve. The parameters of the estimated exponential decay were then used to determine the time at which the curve decayed to 95% decay of its value. This time was reported as the number of steps taken to converge.



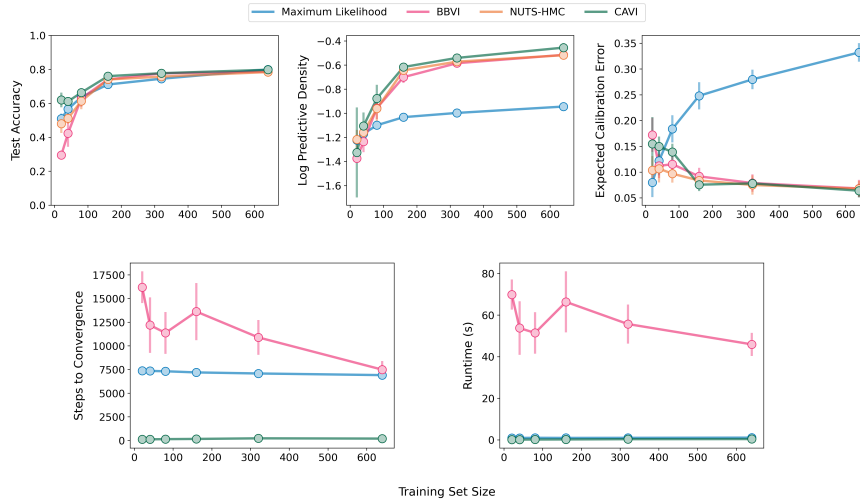


Figure 5: Performance and runtime results of the different models on the ‘Vehicle Silhouettes’ dataset. Descriptions of each subplot are same as in the Figure 2 legend.

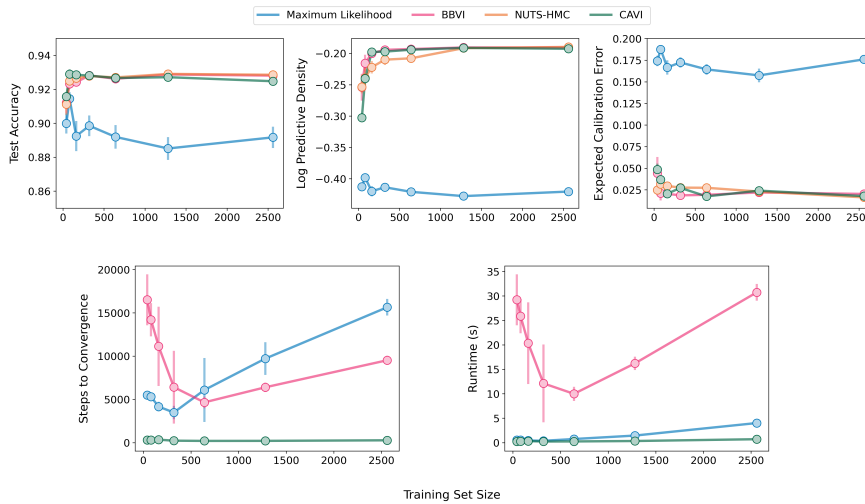


Figure 6: Performance and runtime results of the different models on the ‘Rice’ dataset. Descriptions of each subplot are same as in the Figure 2 legend.

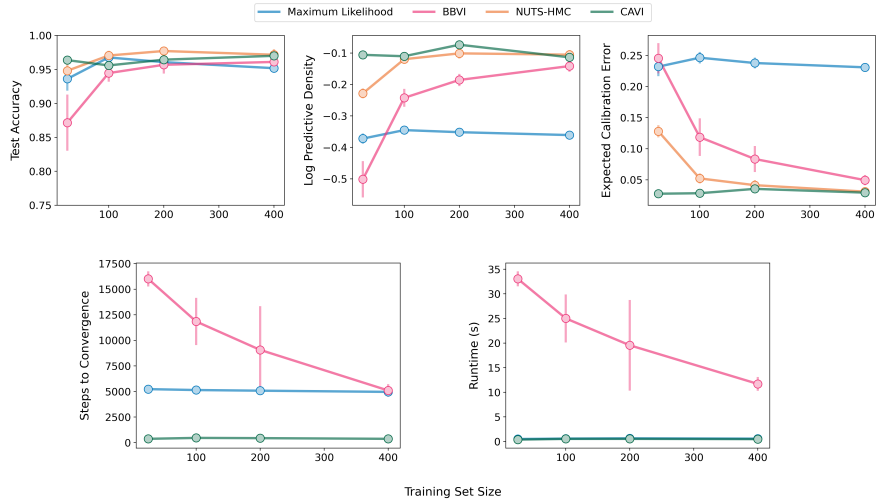


Figure 7: Performance and runtime results of the different models on the 'Breast Cancer' dataset. Descriptions of each subplot are same as in the Figure 2 legend.

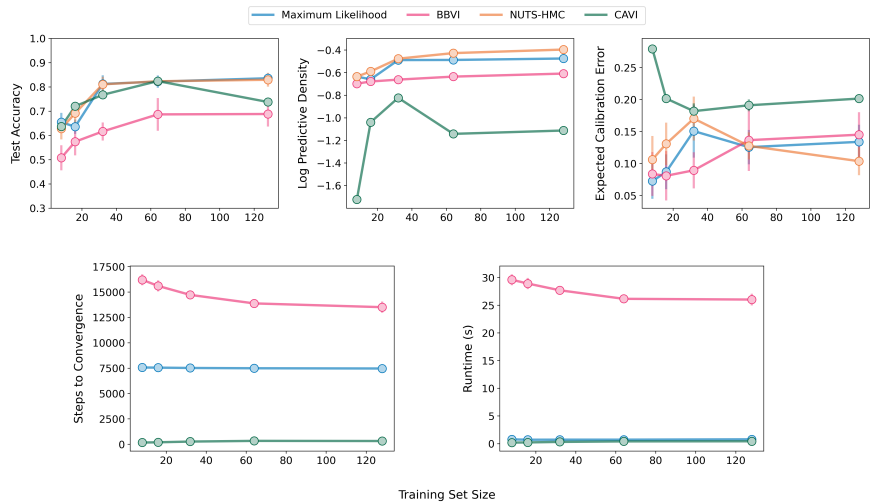


Figure 8: Performance and runtime results of the different models on the 'Connectionist Bench (Sonar, Mines vs. Rocks)' dataset. Descriptions of each subplot are same as in the Figure 2 legend..

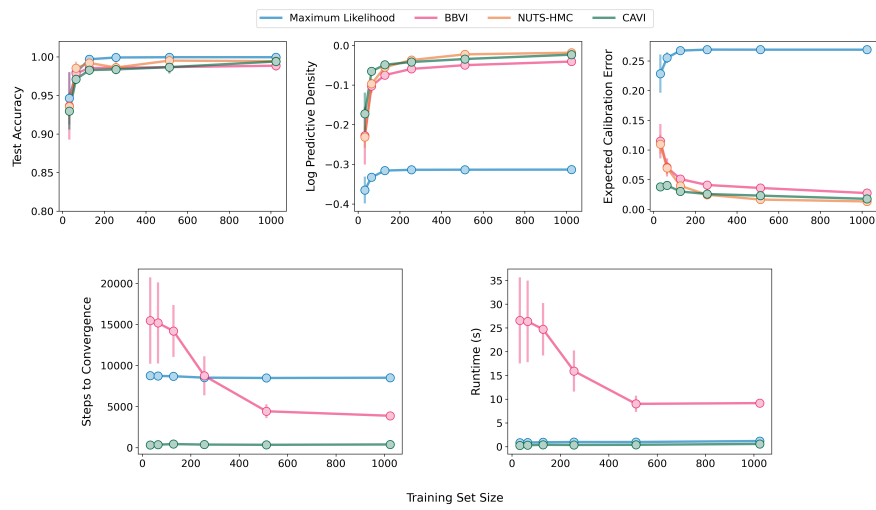


Figure 9: Performance and runtime results of the different models on the 'Banknote Authentication' dataset. Descriptions of each subplot are same as in the Figure 2 legend.